X-ray and ellipsometric study of strong critical adsorption

M. D. Brown,[1] B. M. Law,[1] L. Marchand,[2] L. B. Lurio,[2] I. Kuzmenko,[3] T. Gog,[3] and W. A. Hamilton[4]
[1]*Condensed Matter Laboratory, Department of Physics, Kansas State University, Manhattan, Kansas 66506-2601, USA*
[2]*Department of Physics, Northern Illinois University, DeKalb, Illinois 60115, USA*
[3]*Advanced Photon Source, Argonne National Laboratory, Argonne, Illinois 60439, USA*
[4]*Bragg Institute, Australian Nuclear Science and Technology Organization, Lucas Heights, New South Wales 2234, Australia*
(Received 18 April 2007; published 25 June 2007)

Carpenter *et al.* [Phys. Rev. E **61**, 532 (2000)] succeeded in determining a single universal model, called the P1 model, that could describe the ellipsometric critical adsorption data from the liquid-vapor interface of four different critical binary liquid mixtures near their critical demixing temperatures. The P1 model also recently has been used to describe neutron reflectometry data from a critical liquid mixture/crystalline quartz interface. However, in another recent study, the P1 model failed to simultaneously describe x-ray reflectometry and ellipsometry data from the liquid-vapor surface of the critical mixture *n*-dodecane + tetrabromoethane (DT). In this paper, we resolve this discrepancy between x-ray and ellipsometric data for the DT system. At large length scales (far from the interface) the local concentration is described by the P1 model in order to correctly reproduce the temperature dependence of the ellipsometric data. Close to the interface, however, the molecular structure must be correctly accounted for in order to quantitatively explain the x-ray data. An important conclusion that arises from this study is that neutron or x-ray reflectometry is most sensitive to short-range interfacial structure, but may provide misleading information about long-range interfacial structure. Ellipsometry provides a more accurate measure of this long-range interfacial structure. Complex interfacial structures, possessing both short- and long-range structure, are therefore best studied using multiple techniques.

DOI: 10.1103/PhysRevE.75.061606 PACS number(s): 68.43.−h, 68.35.Rh, 64.60.Fr

I. INTRODUCTION

At the liquid-vapor interface of a binary liquid mixture there will usually be an adsorbed layer in which the component with the lower surface energy at that interface will dominate the composition. Over a length scale on the order of $\sim 10\xi$, where ξ is the composition fluctuation correlation length, the composition profile will decay to the bulk composition. This composition differential between the bulk and the surface is dependent upon the surface field h_1 [1,2], which depends upon the difference in surface energies between the two components. In 1978 Fisher and de Gennes [3] hypothesized that in the case of a binary liquid mixture that was critical with respect to the demixing phase transition, i.e., that would transition from a state of two coexisting phases of different compositions (two-phase region) to a single mixed state (one-phase region) at the critical temperature T_c, this adsorption profile would exhibit interesting universal behavior near T_c. Liu and Fisher [4] were the first to attempt to describe two different experimental systems using a single universal function. Following this seminal work, Carpenter *et al.* [5,6] determined a single universal model, called the P1 model, which could describe the ellipsometric measurements taken over a range of temperatures for four different critical binary liquid systems.

It is important to verify the P1 model using other experimental techniques because the functional form for this (strong) critical adsorption is expected to be widely applicable in other systems [7]. Additionally, the P1 model forms the basis for models that describe more complicated critical binary systems. For example, Cho and Law [8] studied weak critical adsorption, where h_1 was sufficiently small such that saturation of the adsorption layer by one component of the critical binary mixture was incomplete. They successfully described ellipsometric data for a homologous series of mixtures using a model that reduced to the P1 model in the limit when $h_1 \rightarrow \infty$. In another study, Cho and Law [9] described data from systems where one component was strongly polar using a model based upon the P1 model.

Until recently work using other experimental techniques, such as neutron or x-ray reflectometry, has in general failed to validate either the P1 model, or universality for these systems. Brown *et al.* [10] describe a successful attempt to use the P1 model to describe data from neutron reflectometry measurements on the adsorption profile of a critical mixture of D_2O and 3-methylpyridine against a crystalline quartz substrate. Bowers *et al.* [11] performed a similar experiment, and reported results consistent with the P1 model. There is, however, no ellipsometry data on these systems. Here we describe simultaneous analysis of data from two experimental techniques used to study a single critical liquid mixture system. We investigate the liquid-vapor interface of the nonpolar critical mixture *n*-dodecane + tetrabromoethane (DT). Ellipsometry data for this system were taken by Cho, Law, and Gray [12] and used to verify the P1 model. X-ray reflectometry data were taken by Marschand *et al.* [13]. However, their analysis was inconsistent with the P1 model. The reason for the disagreement between x-ray and ellipsometric data was not understood at the time.

II. THEORY

Fisher and de Gennes [3] hypothesized that in the case of a critical binary liquid mixture the decay profile could be modeled with a universal (system-independent) scaling function defined in terms of the surface field h_1 and the dimen-

 ©2007 The American Physical Society

TABLE I. Critical adsorption P1 scaling function (from Ref. [6]).

Model	Phase	$x_{0\pm}$	$c_\pm$	$c_{1\pm}$	$P_{\infty\pm}$	$P_{1\pm}$	$10^4\sigma$
P1	1	1.15	$0.788^{+0.009}_{-0.015}$	−0.245	$0.963^{+0.117}_{-0.201}$	1.437	1.3756
	2	1.15	$1.117^{+0.013}_{-0.021}$	0.169	$0.572^{+0.357}_{-0.152}$	0.533	

sionless length z/ξ, where z is the depth into the liquid. Sufficiently near T_c the correlation length is described by

$$\xi = \xi_0 t^{-\nu}, \tag{1}$$

where $t \equiv |T-T_c|/T_c$ is the reduced temperature and $\nu \simeq 0.632$ [14] is a universal critical exponent. As $h_1 \to \infty$, corresponding to strong critical adsorption, this surface profile loses its dependence on h_1 and simplifies to

$$m_\pm(z) \equiv \phi(z) - \phi_c = M_- t^\beta P_\pm[(z+z_e)/\xi_\pm], \tag{2}$$

where $\phi(z)$ is the relative volume fraction of the component with the lower surface energy, ϕ_c is the bulk critical composition, M_- is a system-dependent parameter, $\beta \simeq 0.328$ [14] is the universal bulk critical exponent describing the coexistence curve, and $P(x)$ is a universal critical composition scaling function. The subscript +(−) refers to the one-(two-)phase region.

There are constraints on the form of $P(x)$. At the critical temperature ($t=0$), $m(x)$ must remain finite and nonzero. Therefore, the factor t^β in Eq. (2) must be canceled by the leading-order term in $P(x)$. Specifically, $P(x)$ must possess the form [3]

$$P_\pm(x) \sim c_\pm x^{-\beta/\nu} \quad \text{as } x \to 0. \tag{3}$$

It is also necessary to prevent $P(x)$ from diverging at $z=0$; this is the purpose of the extrapolation length z_e which appears in Eq. (2). In past ellipsometric work, z_e has been used to define where the profile is saturated by the component possessing the lowest surface energy via the condition that $m_\pm(0)=1$.

For large x, the profile is expected to exhibit exponential decay [4]. In this case, we have

$$P_\pm(x) \sim P_\pm(\infty) + P_{\infty\pm} e^{-x}. \tag{4}$$

The constant $P_\pm(\infty)$ must be chosen such that Eq. (2) describes the bulk composition as $z \to \infty$. For the one-phase region this requires that $m_+(z\to\infty) \to 0$, and therefore

$$P_+(z \to \infty) \equiv P_+(\infty) = 0. \tag{5}$$

In the two-phase region, the coexistence phase diagram is described by $\phi = \phi_c + M_- t^\beta$, thus,

$$P_-(z \to \infty) \equiv P_-(\infty) = 1. \tag{6}$$

The constants $c_\pm$ and $P_{\infty\pm}$ that appear in Eqs. (3) and (4) will be universal because $P_\pm(x)$ is a universal function. An extensive review of previous experimental work investigating the functional form of $P(x)$ can be found in [10] and references therein.

III. P1 MODEL

In 1999 Carpenter *et al.* [5,6] found a universal scaling function (the P1 model) which successfully described the ellipsometric experimental data for four different critical mixtures both above and below T_c. What follows is a description of the P1 model.

Equations (3) and (4) provide only the leading-order terms for $P(x)$. A viable model must provide a more complete description of both the exponential and power law decay regimes where a crossover between these two regimes must occur at some intermediate value of x. For small x, Diehl and Smock [15] suggested that these higher-order terms should take the form

$$P_\pm(x) = c_\pm x^{-\beta/\nu} + c_{1\pm} x^{(1-\beta)/\nu} + c_{2\pm} x^{(2-\beta)/\nu} + c_{3\pm} x^{3-\beta/\nu} + \dots, \tag{7}$$

where the coefficients $c_{i\pm}$ all represent additional universal constants. For large x, Liu and Fisher [4] suggested the form

$$P_\pm(x) = P_\pm(\infty) + P_{\infty\pm} e^{-x} + P_{1\pm} e^{-2x} + P_{2\pm} e^{-3x} + \dots, \tag{8}$$

where $P_{i\pm}$ represent additional universal constants. Carpenter *et al.* used modified versions of Eqs. (7) and (8),

$$\mathrm{P1}_\pm(x) = \begin{cases} c_\pm x^{-\beta/\nu} + c_{1\pm} x^{(1-\beta)/\nu}, & x < x_0, \quad (9) \\ P_\pm(\infty) + P_{\infty\pm} e^{-x} + P_{1\pm} e^{-2x}, & x \geq x_0, \quad (10) \end{cases}$$

where x_0 is a crossover point between small and large x. The name P1 refers to the fact that $c_{1\pm}$ and $P_{1\pm}$ are chosen such that $P(x)$ and its first derivative are continuous at $x=x_0$. The additional constraint that $m(z)$ is continuous at T_c, together with three experimental constraints, leaves the crossover point x_0 as the only adjustable parameter. The values for $c_\pm$, $c_{1\pm}$, $P_{\infty\pm}$, $P_{1\pm}$, and x_0 that provided the best fit to the experimental ellipsometric data are given in Table I. It should be noted that Carpenter *et al.* examined another model where more terms were kept, with additional constraints of continuity for the second and third derivatives at x_0. However, this more complex "P3" model did not describe the experimental ellipsometric results any better than the simplier P1 model [6].

The four systems analyzed by Carpenter *et al.* all had components that were weakly polar. Equation (2) is strictly applicable to simple nonpolar systems. Therefore Cho, Law, and Gray [12] studied the nonpolar critical mixture *n*-dodecane + tetrabromoethane using ellipsometry. The ellipsometric data for this system were well described by the P1 model without requiring any further modification of the model.

Numerous attempts have been made in the past to confirm the universal surface scaling behavior for strong critical adsorption using other experimental techniques, such as neu-

TABLE II. X-ray and optical parameters for the DT critical mixture.

Substance	ε[a]	$10^6\delta$[b]	$10^8\beta$[b]	M_-[c]	ξ_{o+} (nm)[c]	T_c (°C)
n-dodecane (D)	2.019	1.48	0.0974			
1,1,2,2-tetrabromoethane (T)	2.680	4.36	9.04			
Critical mixture (at ϕ_D=0.45)	2.358	3.06	5.01	0.869	0.29	37.5

[a]Optical dielectric constant at wavelength λ=632.8 nm.
[b]From [30].
[c]From [12].

tron and x-ray reflectometry. Results have been mixed, as summarized in [10]. Many experiments not only disagreed with each other but also disagreed with theory. Two recent neutron experiments, however, provided excellent confirmation of theoretical expectations. Bowers *et al.* [11] confirmed both the power law behavior as well as the expected magnitude of the amplitude c_+ for the critical mixture hexane-d_{14} + perfluorohexane against an octadecyl-coated silicon substrate. Brown *et al.* [10] found good agreement between the P1 model and a neutron reflectometry experiment for 3-methylpyridine + D_2O against a crystalline quartz substrate. A disturbing negative result was reported in [13], where, although a novel x-ray inversion procedure provided a consistent description of x-ray reflectometry data for the liquid-vapor surface of the critical mixture DT, the profiles found from this inversion procedure could not explain ellipsometry data from the same mixture. The profiles also failed to clearly show the expected universal scaling behavior. The purpose of this paper is to reconcile these x-ray and ellipsometry data for the DT system with the P1 model.

IV. EXPERIMENTAL METHODS

Sample preparation and experimental methods for the DT system are discussed in [12] and [13]. What follows is a brief summary and some additional details. The sample for x-ray reflectometry was prepared from n-dodecane (99% purity) and 1,1,2,2-tetrabromoethane (Fluka, 98% purity). (The companies and purities of the chemicals, as stated in [13], were erroneously reversed.) A mixture of relative volume fraction of 45% n-dodecane was prepared. Reference [13] states that this composition is within 1% of the critical volume fraction. A more careful analysis of the lever rule [16] and data indicates that in fact this composition is within 0.3% of the critical composition. The sample for ellipsometry was prepared in the same laboratory, under similar conditions [12]. Both samples gave the same ellipsometric results within error bars. Relevant optical and x-ray parameters for the DT critical mixture are listed in Table II.

The x-ray measurements were performed at CNC-CAT at the Advanced Photon Source of Argonne National Laboratory. The sample was in a temperature-controlled environment with a thermal stability of better than 1 mK/h, and thermal gradients of less than 1 mK/cm [17]. The liquid sample was contained within a 7-mm-deep Pyrex trough within a sealed environment. Surface vibrations were dampened by a 19 mm wide ×45 mm long Pyrex table at a level 0.5 mm below the top of the trough. For the DT critical mixture, the n-dodecane component is expected to completely saturate the liquid-vapor surface because this component possesses the lower surface tension. This liquid-vapor surface was maintained at ~0.5 mm above the edges of the trough by overfilling the trough. In this manner, grazing incidence x-ray measurements could be collected while avoiding the experimental complications associated with having a very long sample trough or with passing the x-ray beam through a liquid meniscus [10]. Data were collected at temperatures ranging from 1 to 30 °C above T_c(≃37.5 °C).

The earlier ellipsometry data [12] were collected in a similar temperature-controlled environment. Prior to the x-ray experiment, we confirmed that ellipsometry results collected in the x-ray oven (but with the Pyrex table removed) gave identical ellipsometric results to [12] within error bars.

V. ANALYSIS

As we will see shortly, x-ray reflectometry and ellipsometry provide complementary measures of the local composition $\phi(z)$ [Eq. (2)], where x-ray reflectometry is most sensitive to the short-range structure (immediately adjacent to the surface), whereas ellipsometry is most sensitive to the long-range structure which plays a major role at temperatures close to T_c. It is therefore advantageous, especially for interfaces that possess both short- and long-range structure, to use *both* measurement techniques where a single unique $\phi(z)$ must be found that can describe both data sets. In the following, we first briefly describe what each of these two experimental techniques measure before proceeding to determine the composition profile $\phi(z)$.

A. Ellipsometry

In ellipsometry, we measure the ellipticity $\bar{\rho} \equiv \mathrm{Im}(r_p/r_s)$ at the Brewster angle where r_j is the complex reflection amplitude for polarization j. This measurement is composed of two contributions: an intrinsic contribution $\bar{\rho}_i$ determined by the variation in the local composition profile $\phi(z)$ and an additive capillary wave contribution $\bar{\rho}_c$ [18]. For thin films ($\xi/\lambda_v \ll 1$), $\bar{\rho}_i$ is related to the optical dielectric profile $\varepsilon(z)$ at the surface via the Drude equation [19]

$$\bar{\rho}_i = \frac{\pi}{\lambda_v}\frac{\sqrt{\varepsilon_1+\varepsilon_2}}{\varepsilon_1-\varepsilon_2}\int_{-\infty}^{+\infty}\frac{(\varepsilon(z)-\varepsilon_1)(\varepsilon(z)-\varepsilon_2)}{\varepsilon(z)}dz. \quad (11)$$

Here λ_v (=632.8 nm) is the vacuum wavelength of light used in the experiment while $\varepsilon(z)$ varies between its values in the

incident air [$\varepsilon_1=\varepsilon(-\infty)=1$] and in the reflecting liquid [$\varepsilon_2=\varepsilon(+\infty)$] media (Table II). For *thick films*, Eq. (11) is no longer valid and $\bar{\rho}_i$ must be determined by numerically solving Maxwell's equations. This is in general done by decomposing $\varepsilon(z)$ into dielectric slabs of thickness Δz_i at depth z_i. The electric field boundary conditions at each of the interfaces of the slab are matched in order to numerically solve Maxwell's equations [20]. For *AB* liquid mixtures the local dielectric constant $\varepsilon(z)$ is related to the local composition $\phi(z)$, discussed in Secs. I and II, via the two-component Clausius-Mossotti equation [21]

$$f(\epsilon(z))=\Omega[\phi(z)f(\epsilon_{\mathrm{D}})+(1-\phi(z))f(\epsilon_{\mathrm{T}})], \tag{12}$$

$$f(X)\equiv\frac{X-1}{X+2}, \tag{13}$$

where the volume change on mixing

$$\Omega=\frac{V_D+V_T}{V_{D+T}} \tag{14}$$

is assumed to be 1. Here the subscript D (T) refers to the *n*-dodecane (tetrabromoethane) component. The sensitivity of ellipsometry to strong critical adsorption arises because $\phi(z)$ and, therefore, $\bar{\rho}_i$ is a strong function of the reduced temperature $t=|T_c-T|/T_c$. The additive capillary wave component is reasonably temperature independent [22] and does not provide any information about strong critical adsorption.

B. X-ray reflectometry

X-ray reflectometry measures the fraction R of the incident beam that is reflected from a sample at a wave vector Q,

$$Q=\frac{4\pi\sin\theta}{\lambda_X}\approx\frac{4\pi\theta}{\lambda_X}, \tag{15}$$

where θ is the incident grazing angle, λ_X (=0.113 nm) is the x-ray wavelength, while the approximate form is valid for all practical purposes because θ is small. In the first Born approximation, valid at large scattering vectors away from the critical scattering vector Q_c, the intrinsic contribution to the x-ray reflectivity from the variation in the local composition is [23]

$$R_i(Q)=R_F\left|\frac{1}{\rho(\infty)}\int\frac{d\rho(z)}{dz}e^{iQz}dz\right|^2, \tag{16}$$

where $\rho(z)$ is the local electron density with bulk density $\rho(\infty)$ and $R_F\sim Q^{-4}$ is the Fresnel reflectivity for an infinitely sharp and unstructured interface. In the following we therefore plot the quantity $R(Q)Q^4$ as a function of Q, in order to compensate for the strong Q dependence of R_F. Equation (16) is not valid near the critical scattering vector $Q_c\equiv4\pi\theta_c/\lambda_X$, below which the incident beam is totally reflected.

In analogy to ellipsometry, x-ray reflectometry can alternatively be analyzed by treating the profile as a series of thin slabs of uniform composition, and numerically solving Maxwell's equations. This numerical solution is valid for all scattering vectors Q, unlike Eq. (16). The local refractive index at depth z_j is given by

TABLE III. Fitting parameters.

ΔT (°C)	l_2 (nm)	ϕ_2	l_3 (nm)	ϕ_3	$\sigma_{0,1}$ (nm)	χ^2
1	3.37	0.788 (fixed)	0.78	0.686	0.65	15.8
2	2.72	0.788 (fixed)	0.85	0.693	0.62	17.0
3	3.03	0.788 (fixed)	0.68	0.674	0.71	8.5
5	3.13	0.788 (fixed)	0.85	0.674	0.70	33.5
15	2.63	0.788 (fixed)	0.69	0.611	0.63	35.8
Uniform	3.20	0.788	0.80	0.686	0.65	N/A

$$n(z_j)\approx1-\phi(z_j)(\delta_{\mathrm{D}}-i\beta_{\mathrm{D}})-[1-\phi(z_j)](\delta_{\mathrm{T}}-i\beta_{\mathrm{T}}) \tag{17}$$

where

$$\delta_s=\frac{\lambda_X^2}{2\pi}(D_{\mathrm{SL}})_s,\quad \beta_s=\frac{\lambda_X}{4\pi}\mu_s, \tag{18}$$

and $(D_{\mathrm{SL}})_s$ and μ_s are, respectively, the x-ray scattering length density and absorption coefficient for component s (Table II). Maxwell's equations can be solved either via a series of matrix calculations [20] or by using an iterative technique suggested by Parratt [24,23]. In this work we used the Parratt method for computational efficiency. In this method, the ratio of reflected to incident radiation in each layer, $X_j\equiv R_j/T_j$, is calculated as a function of this same ratio in the layer below:

$$X_j\equiv\frac{R_j}{T_j}=e^{-2ik_{z,j}z_j}\frac{r_{j,j+1}+X_{j+1}e^{2ik_{z,j+1}z_j}}{1+r_{j,j+1}X_{j+1}e^{2ik_{z,j+1}z_j}}, \tag{19}$$

where

$$r_{j,j+1}\equiv\frac{k_{z,j}-k_{z,j+1}}{k_{z,j}+k_{z,j+1}} \tag{20}$$

is the Fresnel reflection coefficient for perpendicular polarization. The starting point for the above iteration is the last (deepest) interface at z_N, where $X_{N+1}=R_{N+1}=0$.

Equations (19) and (20) assume that each interface is perfectly smooth, transitioning from one medium to another over an infinitesimal length scale. In reality an interface j will have some finite thickness σ_j. We account for roughness by replacing $r_{j,j+1}$ in Eq. (19) with

$$\tilde{r}_{j,j+1}=r_{j,j+1}\exp(-2k_{z,j}^2\sigma_j^2). \tag{21}$$

where $\exp(-2k_{z,j}^2\sigma_j^2)$ is the Beckmann-Spizzichino factor [25]. Other factors, such as the Nevot-Croce factor $\exp(-2k_{z,j}k_{z,j+1}\sigma_j^2)$ [26], may be used depending on the nature of the rough surface. Tolan [23] discusses this in more detail. In our case we need only to essentially consider the roughness of the liquid-vapor interface, which will be due largely to capillary wave contributions. $\sigma_{0,1}$ in Table III refers to the roughness of the liquid-vapor interface. We do not include roughness elsewhere in our model, as explained below.

C. Determination of $\phi(z)$

As mentioned earlier, we have found contradictory results as to whether or not the ellipsometric P1 model could or could not describe x-ray/ and neutron reflectometry data for strong critical adsorption. In a neutron reflectometry experiment [10], for a critical mixture of D_2O + 3-methyl-pyridine against a crystalline quartz substrate, Brown *et al.* found that the experimental results were consistent with the P1 model for strong critical adsorption, at least for temperatures close to T_c. However, this agreement required that the quartz substrate be only partially saturated by D_2O with a surface volume fraction of 0.86. The partial saturation was attributed to competing hydrogen bonding of the two liquid components for the quartz surface. For temperatures far from T_c ($\Delta T \gtrsim 5$ °C), the neutron results exhibited deviations from the P1 model, which perhaps were an indication of a crossover to mean field behavior.

This excellent neutron reflectometry agreement with the P1 model should be contrasted with the x-ray reflectometry disagreement with the P1 model [13] found at the liquid-vapor surface of the DT mixture. In this x-ray paper an inversion procedure suggested by Sanyal *et al.* [27] provided composition profiles that provided an excellent description of the x-ray data. However, these composition profiles failed to describe the ellipsometric data from the same interface. These two studies [10,13] provide a clearer picture of what one must do in order to resolve this discrepancy between x-ray and ellipsometry data for the DT mixture at the liquid-vapor surface. X-ray and neutron reflectometry are most sensitive to the near-surface structure which, in wave vector space, occurs at large Q far from the critical wave vector Q_c. This near-surface structure is expected to be fairly *temperature independent*. The far-surface structure, that occurs near Q_c, is less well resolved by x-ray and neutron reflectometry. In fact, the value of Q_c provides a practical upper limit to the length scale of features that neutron or x-ray reflectometry can distinguish within a surface profile. This limit is due to the very low resolution for features larger than $l_{\max}=2\pi/Q_c$. For the critical mixture studied here $Q_c=0.277$ nm^{-1}; and $l_{\max}\simeq 23$ nm; hence, from the temperature dependence of the correlation length [Eq. (1)] x-ray reflectivity curves measured at temperature differences $\Delta T=T-T_c \lesssim 1$ °C will be practically indistinguishable from each other (which is what was found experimentally). In contrast to x-ray and neutron reflectometry, single-wavelength ellipsometry is best at resolving large-scale temperature-dependent features (far from the interface) via the strong temperature dependence of $\bar{\rho}$ near T_c. The small-scale (temperature-independent) features, close to the surface, just provide an additive constant background to the ellipticity $\bar{\rho}$.

In order to describe both the x-ray and ellipsometry data for the DT system the composition profile should have the following properties: (i) close to the surface it should look like the x-ray profile deduced in [13] while (ii) far from the surface it should cross over to the P1 model, in order to reproduce the temperature-dependent ellipsometric data close to T_c. Figure 1 shows the simplest model that we have found that can quantitatively describe both the x-ray and ellipsometric data and is consistent with these short- and long-range composition profile requirements. A pure dodecane monolayer at the surface ($\phi_1=1$, $l_1=0.7$ nm) transitions to the P1 model over a distance of ~4.5 nm (about six monolayers) where two intermediate layers have been inserted between the surface (at $z=0$) and the P1 model (at $z \gtrsim 4.5$ nm). The first intermediate layer has a thickness of $l_2 \sim 3.0\pm0.2$ nm and composition $\phi_2 \simeq 0.79$ while the second intermediate layer has a thickness $l_3 \sim 0.8\pm0.1$ nm and composition $\phi_3 \simeq 0.69$. The extrapolation length z_e in Eq. (2) was chosen such that the P1 model begins to decay from a composition of $\phi_4(z=l_1+l_2+l_3)=\phi_3$. The sudden drop from a $\phi_1=1$ (at the surface) to a $\phi_2 \simeq 0.79$ (in the first intermediate layer) agrees reasonably well with the short-range structure found via the x-ray inversion process in [13], as indicated by the inset in Fig. 1 for $\Delta T=1$ °C. The long-range structure in Fig. 1 is very similar to the P1 model. The dotted lines show the variation in n-dodecane composition as a function of depth z for the pure P1 model at $\Delta T=0.01,1,2,3,5$, and 15 °C, while the solid lines represent the actual large-scale structure selected in the model. The pure P1 model has been offset by a distance of l_2+l_3 to demonstrate the match with our surface layering model. The solid lines agree well with the dotted lines for $z>l_1+l_2+l_3$, with the exception of the $\Delta T=15$ °C data. Note that the profile plots for $\Delta T=0.01$ °C in Fig. 1 are for model comparison only. We do not have x-ray data for that temperature.

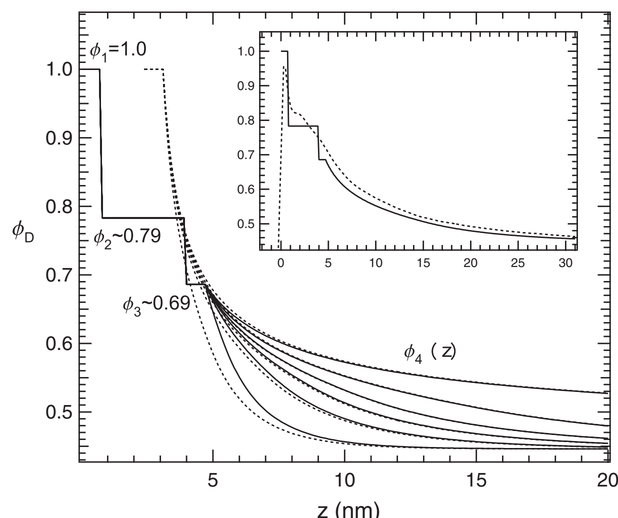

FIG. 1. Plot of the n-dodecane local volume fraction $\phi(z)$ (solid lines) as a function of the depth z away from the liquid-vapor interface at $z=0$ for temperature differences of $\Delta T=0.01,1,2,3,5$, and 15 °C from T_c. The model consists of short-range (temperature-independent) structure consisting of three layers of thickness l_1, l_2, and l_3 with compositions ϕ_1, ϕ_2, and ϕ_3, which joins onto a long-range P1 model at $z=l_1+l_2+l_3$. The long-range structure is very similar to a displaced pure P1 model (dotted lines), at least for $\Delta T \lesssim 5$ °C. Inset: comparison of this model with the x-ray model found via inversion in [13] for $\Delta T=1$ °C.

In obtaining our best fit results we fixed $l_1=0.7$ nm (about one monolayer) for the adsorbed dodecane layer and varied the thicknesses l_2 and l_3, as well as, the compositions ϕ_2 and ϕ_3 of the two intermediate layers. For most fits we found $\phi_2 \approx 0.788$; hence, to limit the parameter space to be

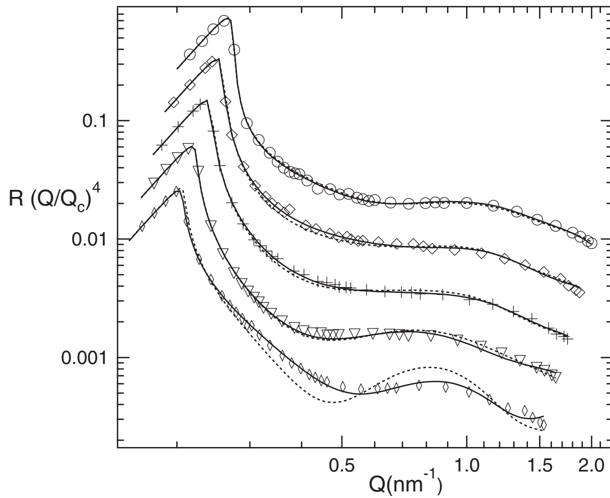

FIG. 2. X-ray reflectometry data taken at $\Delta T=1$ (circles), 2 (diamonds), 3 (pluses), 5 (triangles), and 15 °C (thin diamonds) for the critical mixture *n*-dodecane and 1,1,2,2-tetrabromoethane at the liquid-vapor interface. The solid lines represent fits to the data, as described in the text, where the best fit values for l_2, l_3, ϕ_3, and $\sigma_{0,1}$ are listed in Table III. The experimental data is also compared with a uniform model (dotted lines) where these parameters are fixed at the values given in the last line of Table III. For clarity each curve has been displaced vertically by a factor of 0.07.

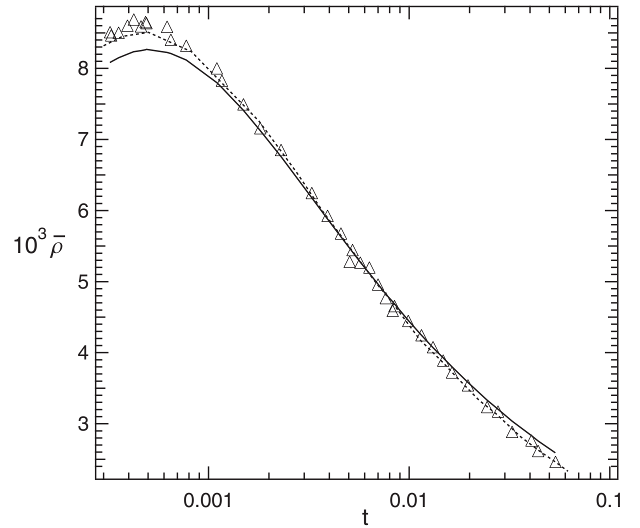

FIG. 3. Ellipsometric data (symbols) collected from the liquid-vapor surface of the critical mixture *n*-dodecane +1,1,2,2-tetrabromoethane as a function of the reduced temperature *t*. Pure P1 model (dotted line). Uniform P1 model (solid line) where the values for l_2, l_3, ϕ_3, and $\sigma_{0,1}$ are listed in Table III.

searched we fixed ϕ_2 at this value. The best fit values for l_2, l_3, ϕ_3, and $\sigma_{0,1}$ were obtained by minimizing

$$\chi^2 = \sum_{i=1}^{N} \frac{[R_{\text{model}}(Q_i) - R_i]^2}{w_i^2}, \tag{22}$$

where R_i represents the experimental x-ray reflectivity data at wave vector Q_i while $R_{\text{model}}(Q_i)$ corresponds to the x-ray reflectivity for our model. In carrying out this fitting procedure one must take particular care in selecting the weight w_i for each data point [10]. If the standard weight $w_i = \sqrt{R(Q_i)}$ is selected then the high-Q data points have insufficient impact on the overall fit, thus leading to an inaccurate picture of the profile. This difficulty arises because the reflectivity decreases by several orders of magnitude for increasing Q above Q_c. One must also be careful not to overweight the higher-Q data points because then the fit becomes susceptible to the noise in the higher-Q data. The weighting factor [10]

$$w_i = R(Q_i)\sqrt{1 - \log_{10}[R(Q_i)]} \tag{23}$$

was found to give results that were consistent over the entire Q range. The first term in Eq. (23) $[R(Q_i)]$ compensates for the differing orders of magnitude in the reflectivity between low- and high-Q data while the second term decreases the weighting for the noisier higher-Q data.

The best fit values obtained for l_2, l_3, ϕ_3, and $\sigma_{0,1}$ are listed in Table III where this model (solid lines) is compared with the x-ray data (symbols) in Fig. 2. We expect that the short-range structure encompassed by the parameters l_2, l_3, ϕ_3, and $\sigma_{0,1}$ should be fairly temperature independent, at least for temperatures close to T_c, where $\sigma_{0,1}$ should be similar in magnitude to the value found at the liquid-vapor surface of long *n*-alkane liquids [28]. This is indeed found to be approximately true from the results in Table III. Therefore, we have also considered a model where l_2, l_3, ϕ_3, and $\sigma_{0,1}$ are fixed at the values given in the last line of Table III. This uniform model is also compared with the x-ray data in Fig. 2 (dotted lines). With the exception of the $\Delta T=15$ °C, the uniform model provides an excellent description of the x-ray data. The uniform model also provides a reasonable description of the ellipsometric data $\bar{\rho}$ as a function of the reduced temperature t (Fig. 3) where the dotted line is the pure P1 model while the solid line is the uniform model.

As mentioned above, we explicitly included roughness at the liquid-vapor interface via the parameter $\sigma_{0,1}$. We do not, however, include roughness below either the first or second intermediate layers. Doing so would add two additional roughness parameters $\sigma_{1,2}$ and $\sigma_{2,3}$ to our model. If one includes $\sigma_{1,2}$ and $\sigma_{2,3}$ in our model, similar fits to the x-ray and ellipsometry data are obtained without gaining any additional insight into the universal critical behavior.

Our layering scheme does overstate the ellipsometric background term by 1.2×10^{-3} as compared to the data taken by Cho, Law, and Gray [12]. A more sophisticated model than the one we present here may be able to account for much of this. However, this shift is not much larger than typical differences we see between ellipsometric measurements on different samples of the same binary liquid system. For example, the ellipsometric data we took to compare our results to those of Cho, Law, and Gray [12] resulted in a background term 0.4×10^{-3} higher than theirs.

The neutron experiment in [10] suggests that only ellipsometric and x-ray data at $\Delta T \lesssim 5$ °C can be expected to be well explained by the P1 model, which incorporates Ising critical exponents where critical fluctuations play a dominant role. At $\Delta T \gtrsim 5$ °C a crossover to mean field behavior might be expected [29]; this is probably the explanation for the

difference between the uniform model and experimental x-ray data at $\Delta T = 15\ ^\circ\mathrm{C}$ in Fig. 2.

VI. CONCLUSION

In this paper we have found a model that successfully describes both the Q and temperature dependence of the x-ray reflectivity data (Fig.2), as well as the temperature dependence of the ellipsometric data (Fig. 3) for strong critical adsorption of n-dodecane at the liquid-vapor surface of the critical mixture n-dodecane + 1,1,2,2-tetrabromoethane. This model consisted of large depth z structure described by the P1 model, used in ellipsometry, where short-range temperature-independent z structure was added to this model (Fig. 1). Good agreement is found between theory and experiment at least for temperatures within $5\ ^\circ\mathrm{C}$ of T_c. At larger temperatures, further from T_c, this model does not describe experimental data as well—a fact that we attribute to a crossover to mean field behavior. This study illustrates the utility of combining x-ray or neutron reflectometry (to deduce short-range interfacial structure) with ellipsometry (to study long-range interfacial structure). Such a combination of experimental techniques will be important for ascertaining the interfacial behavior of complex surfaces that possess features on many different length scales.

ACKNOWLEDGMENTS

Two of the authors (B.M.L. and L.L.) acknowledge support for this work from the U.S. Department of Energy through Grant No.DE-FG02-02ER46020. B.M.L. also acknowledges partial support through National Science Foundation Grant No. DMR-0603144. The Advanced Photon Source at Argonne National Laboratory is supported by DOE Grant No. W-31-109-Eng-38.

[1] M. E. Fisher and H. Au-Yang, Physica A **101**, 255 (1980); H. Au-Yang and M. E. Fisher, Phys. Rev. B **21**, 3956 (1980).
[2] U. Ritschel and P. Czerner, Phys. Rev. Lett. **77**, 3645 (1996).
[3] M. E. Fisher and P.-G. de Gennes, C. R. Seances Acad. Sci., Ser. B **287**, 207 (1978).
[4] A. J. Liu and M. E. Fisher, Phys. Rev. A **40**, 7202 (1989).
[5] J. H. Carpenter, B. M. Law, and D. S. P. Smith, Phys. Rev. E **59**, 5655 (1999).
[6] J. H. Carpenter, J.-H. J. Cho, and B. M. Law, Phys. Rev. E **61**, 532 (2000).
[7] H. W. Diehl, Int. J. Mod. Phys. B **11**, 3503 (1997).
[8] J.-H. J. Cho and B. M. Law, Phys. Rev. Lett. **86**, 2070 (2001);Phys. Rev. E **65**, 011601 (2001).
[9] Jae-Hie J. Cho and B. M. Law, Phys. Rev. Lett. **89**, 146101 (2002); Phys. Rev. E **67**, 031605 (2003).
[10] M. D. Brown, B. M. Law, S. Satija, W. A. Hamilton, E. Watkins, J.-H. J. Cho, and J. Majewski, J. Chem. Phys. (to be published).
[11] J. Bowers, A. Zarbakhsh, H. K. Christenson, I. A. McLure, J. R. P. Webster, and R. Steitz, Phys. Rev. E **72**, 041606 (2005).
[12] J.-H. J. Cho, B. M. Law, and K. Gray, J. Chem. Phys. **116**, 3058 (2002).
[13] L. W. Marschand, M. Brown, L. B. Lurio, B. M. Law, S. Uran, I. Kuzmenko, and T. Gog, Phys. Rev. E **72**, 011509 (2005).
[14] M. E. Fisher and J.-H. Chen, J. Phys. (Paris) **46**, 1645 (1985).
[15] H. W. Diehl and M. Smock, Phys. Rev. B **47**, 5841 (1993); **48**, 6470(E) (1993).
[16] L. D. Landau and E. M. Lifshitz, *Statistical Physics*, 3rd ed. (Pergamon, Oxford, 1980), Part 1.
[17] M. Brown, S. Uran, B. Law, L. Marschand, L. Lurio, I. Kuzmenko, and T. Gog, Rev. Sci. Instrum. **75**, 2536 (2005).
[18] A. M. Marvin and F. Toigo, Phys. Rev. A **26**, 2927 (1982).
[19] P. K. L. Drude, *The Theory of Optics* (Dover, New York, 1959), p. 292.
[20] M. Born and E. Wolf, *Principle of Optics* (Pergamon, Oxford, 1980), Sec. 1.6.
[21] R. F. Kayser, Phys. Rev. B **34**, 3254 (1986).
[22] D. S. P. Smith and B. M. Law, Phys. Rev. E **54**, 2727 (1996).
[23] M. Tolan, *X-Ray Scattering from Soft-Matter Thin Films* (Springer-Verlag, New York, 1999).
[24] L. G. Parratt, Phys. Rev. **95**, 359 (1954).
[25] P. Beckmann and A. Spizzichino, *The Scattering of Electromagnetic Waves from Rough Surfaces* (Pergamon, New York, 1963).
[26] L. Nevot and P. Croce, Rev. Phys. Appl. **15**, 761 (1980).
[27] M. K. Sanyal, S. Hazra, J. K. Basu, and A. Datta, Phys. Rev. B **58**, R4258 (1998).
[28] B. M. Ocko, X. Z. Wu, E. B. Sirota, S. K. Sinha, and M. Deutsch, Phys. Rev. Lett. **72**, 242 (1994).
[29] J. K. Whitmer, S. B. Kiselev, and B. M. Law, J. Chem. Phys. **123**, 204720 (2005).
[30] http://www.cxro.lbl.gov/opticalconstants/getdb2.html.